A helix-breaking mutation in TRPML3 leads to constitutive activity underlying deafness in the varitint-waddler mouse

Christian Grimm*, Math P. Cuajungco*†, Alexander F. J. van Aken‡, Michael Schnee*, Simone Jörs*, Corné J. Kros‡, Anthony J. Ricci*, and Stefan Heller*§

*Departments of Otolaryngology, Head and Neck Surgery, and Molecular and Cellular Physiology, Stanford University School of Medicine, Stanford, CA 94305; and ‡School of Life Sciences, University of Sussex, Brighton BN1 9QG, United Kingdom

Communicated by A. James Hudspeth, The Rockefeller University, New York, NY, October 16, 2007 (received for review August 6, 2007)

Homozygote varitint-waddler (*Va*) mice, expressing a mutant isoform (A419P) of TRPML3 (mucolipin 3), are profoundly deaf and display vestibular and pigmentation deficiencies, sterility, and perinatal lethality. Here we show that the varitint-waddler isoform of TRPML3 carrying an A419P mutation represents a constitutively active cation channel that can also be identified in native varitint-waddler hair cells as a distinct inwardly rectifying current. We hypothesize that the constitutive activation of TRPML3 occurs as a result of a helix-breaking proline substitution in transmembrane-spanning domain 5 (TM5). A proline substitution scan demonstrated that the inner third of TRPML3's TM5 is highly susceptible to proline-based kinks. Proline substitutions in TM5 of other TRP channels revealed that TRPML1, TRPML2, TRPV5, and TRPV6 display a similar susceptibility at comparable positions, whereas other TRP channels were not affected. We conclude that the molecular basis for deafness in the varitint-waddler mouse is the result of hair cell death caused by constitutive TRPML3 activity. To our knowledge, our study provides the first direct mechanistic link of a mutation in a TRP ion channel with mammalian hearing loss.

cation channel | cochlea | hair cell | inner ear | TRP channel

Transient receptor potential (TRP) cation channels are important components of many cellular and sensory systems, such as osmosensation, photosensation, taste sensation, and thermosensation (1, 2). In *Drosophila*, *Caenorhabditis elegans*, and lower vertebrates, mutations in TRP channels have also been associated with loss of sensitivity to touch and other forms of mechanical stimulation (3–5). Besides the general notion that they conduct cations, TRP channels have quite diverse structural and functional properties (1, 2).

The identification of mutations in the human mucolipin (*TRPML1*) gene as the cause of mucolipidosis type IV, a neurodegenerative, recessive, lysosomal storage disorder characterized by psychomotor retardation and visual impairment, led to the initial description of the TRPML subfamily (6, 7). The mammalian TRPML subfamily consists of three members: TRPML1, TRPML2, and TRPML3. Like other TRP channels TRPML proteins contain six putative transmembrane domains with cytosolic amino and carboxyl termini. A mutant isoform of murine *Trpml3* has recently been identified as the underlying cause of the varitint-waddler (*Va*) phenotype that is manifested in profound deafness, vestibular defects, pigmentation deficiencies, sterility, and perinatal lethality (8, 9). The *Trpml3* (*Va*) allele displays an alanine to proline substitution at amino acid position 419 (A419P) in the fifth transmembrane domain of TRPML3 (8) [supporting information (SI) Fig. 5]. A second amino acid substitution (I362T) positioned at the second extracellular loop arose in *cis* to A419P, resulting in the Va^J allele that attenuates and partially rescues the severe *Va* phenotype by an unknown mechanism.

The present work was conducted to determine the specific role of the varitint-waddler A419P substitution on TRPML3 by examining the mutation's physiological and molecular effects using both *in vitro* and *in vivo* approaches. Our study linked the A419P mutation of TRPML3 with a hot spot in TM5 for helix-breaking (10) mutations causing constitutively active channels. This potential site for constitutively activating mutations is not restricted to TRPML3 but includes all three mucolipins and surprisingly also extends to TRPV5 and TRPV6, suggesting that these five channels potentially share certain structure–function similarities.

Results

A419P Turns TRPML3 into a Constitutively Active Cation Channel Leading to Cell Death. When murine and human TRPML3 as well as the corresponding varitint-waddler mutant isoforms were expressed in HEK293 cells, those cells expressing TRPML3(A419P) (*Va*) or TRPML3(I362T/A419P) (Va^J) displayed significantly elevated $[Ca^{2+}]_i$ and $[Na^+]_i$ when compared with wild-type TRPML3- or TRPML3(I362T)-expressing cells (Fig. 1 *A* and *B*). The I362T mutation that moderately attenuates the A419P phenotype in Va^J mice (8) did not significantly ameliorate the influx of cations through A419P-mutated TRPML3. The increased $[Ca^{2+}]_i$ caused by the A419P mutation depended on influx of extracellular Ca^{2+} (Fig. 1 *C* and *D*).

We next tested whether the increased $[Ca^{2+}]_i$ of cells that express the (*Va*) or (Va^J) isoforms of TRPML3 resulted in detrimental cellular changes. Already 10 h after transfection, we determined that 20–30% of TRPML3(A419P)- and TRPML3(I362T/A419P)-expressing cells were annexin V-positive, an indicator of early apoptosis (Fig. 1*E*). Within the next 15 h, the number of annexin V-positive cells increased to 70%. We conclude that massive Ca^{2+} influx causes apoptosis in cells expressing TRPML3(A419P) or TRPML3(I362T/A419P).

Whole-cell patch clamp analysis showed that TRPML3(A419P) and TRPML3(I362T/A419P) displayed a constitutively active conductance that had a significant portion of the conductance active at the cell's resting potential, which was not detectable with wild-type TRPML3 (Fig. 2 *A* and *B*). The current–voltage (I/V) plots appear inwardly rectified. Whether this is voltage-dependent channel closure or a property of channel permeation remains to be determined because the lack of detectable activation or deactivation kinetics at any potential

Author contributions: C.G., M.P.C., A.J.R., and S.H. designed research; C.G., M.P.C., A.F.J.v.A., M.S., S.J., C.J.K., and A.J.R. performed research; C.G., M.P.C., A.F.J.v.A., M.S., S.J., C.J.K., A.J.R., and S.H. analyzed data; and C.G., M.P.C., A.J.R., and S.H. wrote the paper.

The authors declare no conflict of interest.

†Present address: Department of Biological Sciences, California State University, 800 North State College Boulevard, Fullerton, CA 92831.

§To whom correspondence should be addressed. E-mail: hellers@stanford.edu.

This article contains supporting information online at www.pnas.org/cgi/content/full/0709846104/DC1.

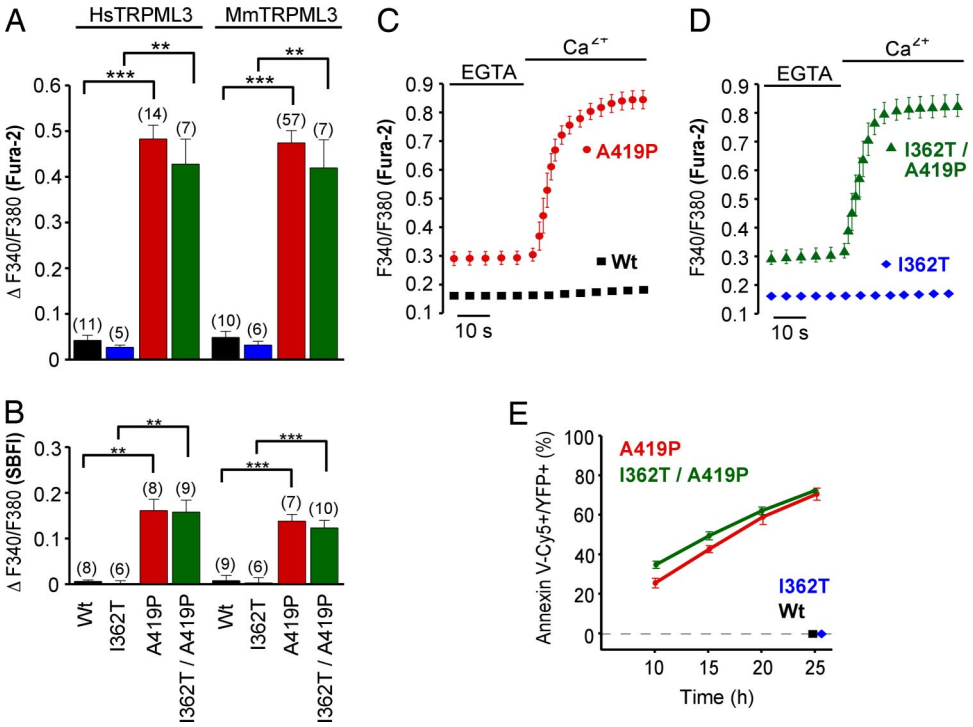

Fig. 1. Elevated intracellular Ca^{2+} and Na^+ levels and annexin V binding to HEK293 cells expressing varitint-waddler TRPML3 mutants. Ca^{2+} imaging (*A*) and Na^+ imaging (*B*) results showing intracellular Ca^{2+} and Na^+ levels of HEK293 cells expressing human (Hs) and murine (Mm) TRPML3 and the respective mutants. All experiments were performed 10–15 h after transfection (mean ± SEM; *n* is in parentheses. ***, $P < 0.0001$; **, $P < 0.001$ (Student's *t* test, unpaired, comparison with wild type). Transfected cells were identified by YFP fluorescence of the expressed proteins. (*C* and *D*) Ca^{2+} imaging experiments showing that the $[Ca^{2+}]_i$ increase depends on extracellular Ca^{2+}. After incubation in 2 mM EGTA for 5 min, the external buffer solution was switched to 2 mM calcium. (*E*) Quantification of the number of transfected HEK293 cells that bound Cy5-conjugated annexin V, an indication of early signs of apoptosis. Shown are time points after transfection with expression vectors for the mutants indicated. We found no annexin V-positive cells expressing wild-type TRPML3 or TRPML3(I362T) 25 h after transfection.

made interpretations difficult. At positive potentials there was a large outward transient suggesting that a channel block creates the rectification in the I/V curve. The simplest interpretation of these records is that the mutation leaves the channel in an open unregulated state and that outward permeation is blocked in a non-voltage-dependent manner. Currents normalized to the steady-state current elicited at −200 mV revealed no significant difference in the I/V relationships between the two mutant TRPML3 alleles (Fig. 2*C*).

Based on the finding that the currents generated by the A419P mutation in HEK293 cells were the same as those generated by the I362T/A419P mutation, it remained unclear what might explain the difference in phenotype between mice with these mutations. To determine whether the mutations altered the plasma membrane localization of TRPML3, biotinylation experiments were performed. Surface biotinylation revealed that the I362T/A419P mutation resulted in a significant reduction of the mutated TRPML3 protein in the plasma membrane when compared with the A419P mutant isoform [35% reduction from 6.0 ± 0.8% to 3.9 ± 0.6% ($P = 0.04$); wild-type TRPML3, 24.8 ± 2.4% (mean ± SEM); $n = 4$] (SI Fig. 6). According to this, fewer channels in the plasma membrane probably account for the slightly milder phenotype of the (Va^J) varitint-waddler allele.

Analysis of the electrophysiological properties of varitint-waddler (Va^J/Va^J) mouse cochlear outer hair cells (OHCs) revealed a distinct inwardly rectifying conductance not detectable in wild-type OHCs that was activated at rest (Fig. 2 *D–F*). The I/V relationship showed remarkable overlap for the inward component for the OHC conductance compared with that of expressed TRPML3(I362T/A419P) in HEK293 cells. The inwardly rectifying conductance of (Va^J/Va^J) OHCs did not differ significantly from the currents elicited in HEK293 cells by TRPML3(A419P) or TRPML3(I362T/A419P) (Fig. 2*G*), suggesting that the (Va^J/Va^J) phenotype is caused by constitutively active TRPML3. The transient outward component was not observed in the outer hair cell recordings.

A419P Is a Classic Helix-Breaking Mutation. The varitint-waddler phenotype-causing mutation in TRPML3 is a substitution of alanine at position 419 with a proline. Introduction of a proline into an α-helix often causes kinks or swivels in the generally noncompliant helical structure (10). Glycine can have a similar but milder effect (10, 11). We tested whether substitution of A419 with other amino acids of distinctive chemical features affected TRPML3. We found that A419P and, to a lesser extent, A419G were the only changes causing elevation of $[Ca^{2+}]_i$ (Fig. 3*A*). Substitutions of the adjacent alanine at position 420 did not result in increased $[Ca^{2+}]_i$. All mutants displayed subcellular distribution similar to wild-type TRPML3 (SI Fig. 7), indicating that protein mislocalization was not responsible for the measured responses. These results suggest that the introduction of an α-helix-breaking kink or swivel at position 419 in TM5 causes a structural change, converting TRPML3 into a constitutively open cation channel. We further investigated the effect of helix-breaking prolines on TM5 by conducting a proline substitution scan, and we found that introduction of a single proline at any position from amino acids 413 to 419, which is the intracellularly oriented third of TM5, led to increased $[Ca^{2+}]_i$ in transfected HEK293 cells (Fig. 3*B*). Besides this region of susceptible residues, G425P and C429P mutations also displayed significantly elevated $[Ca^{2+}]_i$. A few of the unaffected mutant isoforms of TRPML3 displayed reduced plasma membrane

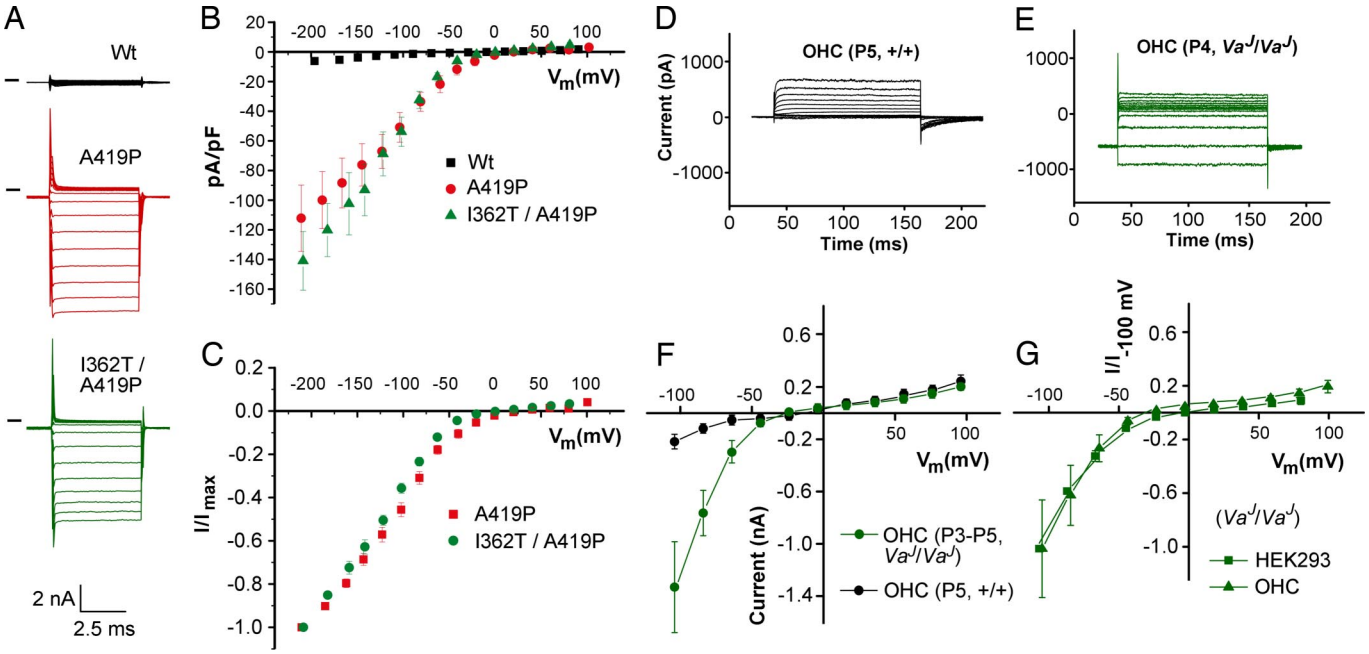

Fig. 2. Constitutively active conductance elicited by varitint-waddler TRPML3 mutants in HEK293 cells and cochlear outer hair cells. (*A*) Currents elicited from wild type (black), A419P mutant (red), and I362/A419P mutant (green) in response to 5-ms voltage steps from a holding potential of −50 mV between −200 mV and +100 mV in 20-mV incremental steps. Black bars indicate zero current line. (*B*) Steady-state current–voltage plots from *A* normalized to cell capacitance. A two-tailed Student *t* test revealed no significant difference ($P > 0.01$) between the data points for any voltage measured ($n = 9$ for A419P, and $n = 9$ for I362T/A419P). (*C*) Same plot, but normalized to maximal current elicited at −200 mV to demonstrate similarity in responses. (*D*) Currents from a wild-type outer hair cell measured with Cs^+-based intracellular solution. Membrane voltage range: −104 mV to +96 mV, in 20-mV increments, from a holding potential of −84 mV. (*E*) Currents recorded from a Va^J/Va^J outer hair cell under the same conditions as in *D*. (*F*) Comparison of the current–voltage curves for experiments similar to those shown in *D* and *E*, determined just after the start of the voltage steps. Conductance at −84 mV was 1.95 ± 0.26 nS for wild type ($n = 4$ OHCs, mean ± SEM) and 28.0 ± 7.4 nS for Va^J/Va^J ($n = 7$ OHCs) ($P < 0.02$, unpaired *t* test). (*G*) Normalized hair cell current from Va^J/Va^J mouse OHCs ($n = 7$) compared with expressed I362T/A419P ($n = 9$), normalized to −100 mV, to demonstrate similarity between responses. No statistical differences were found between the outer hair cell currents and the expressed currents at any voltage using the Student two-tailed *t* test ($P > 0.05$).

localization as judged by confocal microscopy (data not shown) and surface biotinylation (Fig. 3*C*). Overall, however, there was no correlation of reduced plasma membrane localization with insensitivity to proline substitution. Several of the mutant TRPML3 channels were tested by whole-cell recordings revealing isoforms that exhibited increased $[Ca^{2+}]_i$ to also have constitutively open channels very similar to TRPML3(A419P) (Fig. 3 *D–F*).

TM5 Susceptibility Is a General Feature of TRPMLs as Well as TRPV5 and TRPV6. The substantial susceptibility of TRPML3's TM5 to helix-breaking mutations led us to explore whether other TRP channels display a similar propensity. Via sequence alignments we identified positions equivalent to A419 in TRPML1, TRPML2, TRPV5, TRPV6, TRPV2, TRPM2, and TRPC6 (Fig. 4*A*). We replaced the amino acids at these positions with a proline, and we compared the $[Ca^{2+}]_i$ of HEK293 cells transfected with the mutant isoforms with their respective wild type-expressing cells. We found that cells expressing TRPML1(V432P), TRPML2(A396P), TRPV5(M490P), and TRPV6(M497P) all exhibited elevated $[Ca^{2+}]_i$ when compared with their respective wild-type isoforms (Fig. 4*B*). TRPV2(Y539P), TRPM2(L941P), and TRPC6(F641P) did not evoke increased $[Ca^{2+}]_i$. We further mutated TRPV2, TRPM2, and TRPC6 at additional positions in TM5 whose equivalent substitutions caused increased $[Ca^{2+}]_i$ of TRPML3 mutants, and none of these mutant isoforms displayed elevated $[Ca^{2+}]_i$ when compared with the respective wild-type channels (Fig. 4*C* and SI Fig. 8*A*). All TRPV2, TRPM2, and TRPC6 proline mutants generated showed subcellular localization identical to their respective wild-type channels (SI Fig. 8*B*). To exclude that the individual proline substitutions led to channel inactivation, functional tests of the mutant channels were performed by using specific agonists. TRPV2 mutants were gated with diphenyl boronic anhydride (DPBA) (12), and TRPC6 mutants were gated with 1,2-didecanoyl-glycerol (DDG) (13, 14) in calcium imaging experiments; TRPM2 mutant gating was tested in patch-clamp experiments using ADP-ribose (15, 16) (SI Fig. 8 *C–E*). Some of the investigated mutant channel isoforms displayed decreased responsiveness [TRPV2(Y539P), TRPV2(G545P), and TRPC6(F641P)].

The considerable effect of the M490P and M497P substitutions on TRPV5 and TRPV6 suggested that these two channels display a susceptibility of TM5 to helix-breaking mutations similar to TRPML channels. We proline-scanned TM5 of TRPV5 and found that, similar to TRPML3, introduction of prolines into the intracellularly oriented third of TRPV5 resulted in massive influx of Ca^{2+} (Fig. 4*D*). Some mutations displayed $[Ca^{2+}]_i$ levels similar to wild-type TRPV5, and several mutants showed reduced $[Ca^{2+}]_i$ when compared with wild type, which could be a consequence of reduced plasma membrane expression (data not shown) or an indication of inactivity of the respective mutant channel isoform.

Discussion

The most apparent observation that we made when expressing TRPML3(A419P) or TRPML3(I362T/A419P) in HEK293 cells was the massive increase of $[Ca^{2+}]_i$ leading to apoptosis. The electrophysiological analysis corroborated the Ca^{2+} imaging results revealing an inwardly rectifying current in HEK293 cells expressing either TRPML3(A419P) or TRPML3(I362T/A419P). Similar currents were observed in outer hair cells of homozygous

NEUROSCIENCE

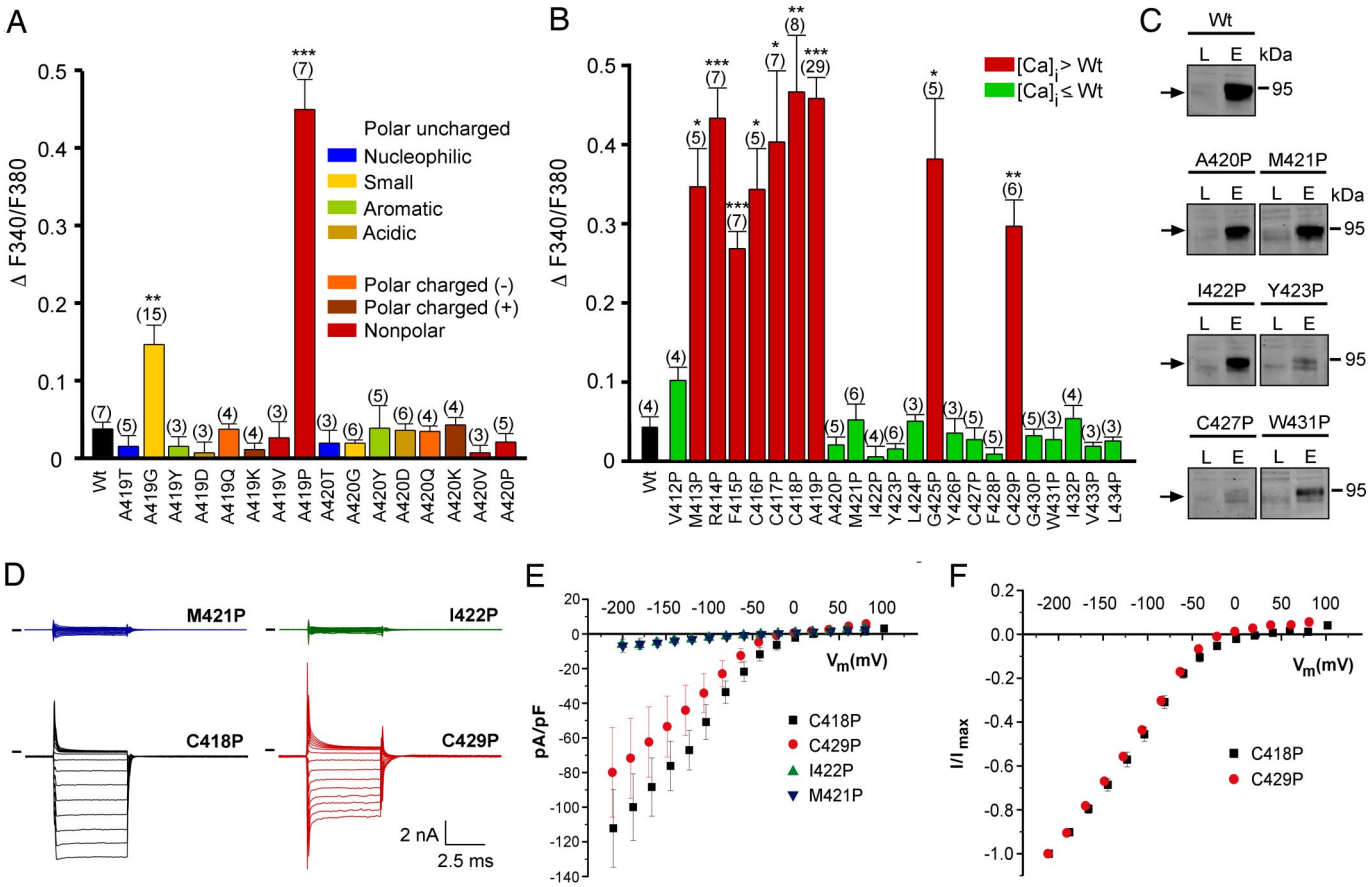

Fig. 3. Effects of amino acid substitutions in TM5 of TRPML3. (*A*) Effect of the substitution of alanine at positions 419 and 420 in murine TRPML3 by various amino acids on $[Ca^{2+}]_i$. Note that only proline and glycine substitution at position 419 significantly led to an increase of $[Ca^{2+}]_i$. Shown are mean values ± SEM with *n* in parentheses. All experiments were performed 10–15 h after transfection. (*B*) Effect on $[Ca^{2+}]_i$ of proline substitution of the residues predicted to constitute TM5 of murine TRPML3. Shown are mean values ± SEM with *n* in parentheses. Nine (red) of the 23 mutant isoforms showed significantly elevated basal intracellular calcium levels compared with wild-type TRPML3 (Wt). V412P is not part of the predicted TM5. ***, $P < 0.0001$; **, $P < 0.001$; *, $P < 0.01$ (Student's *t* test, unpaired, comparison with wild type). (*C*) Surface biotinylation analysis. TRPML3 wild-type protein (Wt) and the mutant isoforms are present in the plasma membrane. L indicates input load (1% of total), and E indicates elution from neutravidin beads of surface-biotinylated TRPML3 visualized by Western blot. (*D*) Voltage-clamp recording from mutants as listed, expressed in HEK293 cells. Voltage protocol consists of 20-mV incremental steps between −200 and +80 mV. Inward rectifier current is present in mutant TRPML3-expressing cells that showed elevated calcium and is not present in those where calcium was not elevated. Black bars indicate zero current line. (*E*) Steady-state current–voltage plots generated from data in *D*. (*F*) Current–voltage plots normalized to current at −200 mV to demonstrate similar relationships between mutants.

Va^J/*Va*^{J} mice, indicating that cochlear varitint-waddler hair cells experience cation influx through the mutated TRPML3 channel.

Approximately 75% of TRPML3 protein is located in intracellular compartments of transfected HEK293 cells. The remaining 25% of the total TRPML3 protein is localized in the plasma membrane. Studies of TRPML3 expression in hair cells revealed TRPML3 localization in both intracellular compartments and associated with the plasma membrane (8). The same study reported differences in severity between the *Va* and *Va*^{J} phenotypes, which might be a result of the 35% reduced plasma membrane localization of the TRPML3(I362T/A419P) channel when compared with TRPML3(A419P).

Overall, it is remarkable that cochlear hair cells are able to survive the presence of the TRPML3(I362T/A419P)-mediated current for several postnatal weeks, whereas other cells, such as the cochlear melanocytes, degenerate before birth (9). TRPML3(A419P)- or TRPML3(I362T/A419P)-expressing HEK293 cells were not able to survive for >24 h, which is probably partially a result of the artificial overexpression in this heterologous system. The prolonged resistance of inner and outer hair cells may be the result of a combination of circumstances. A potential factor is the substantial reduction of the endocochlear potential in homozygous *Va*^{J}/*Va*^{J} mice, attributed to missing melanocytes (intermediate cells) in the *stria vascularis* (9), which substantially reduces the driving force for cations into cochlear hair cells. Another contributing factor may be the inherent ability of hair cells to deal with massive Ca^{2+} loads, which is manifested by the high cytosolic concentration of various calcium buffers (17–19) and by the presence of high concentrations of PMCA-type calcium pumps in their stereociliary bundles (20, 21).

The introduction of proline substitutions into TM5 of other TRP channels revealed an unexpected potential structural relationship of TRPML channels with TRPV5 and TRPV6. Our Ca^{2+} imaging analysis revealed that HEK293 cells expressing the mutant channels displayed significantly elevated $[Ca^{2+}]_i$ levels when compared with the respective wild type-expressing cells. Although intriguing, it is not clear whether the mechanisms leading to increased $[Ca^{2+}]_i$ levels in mutant TRPV5 and TRPV6 are the same as in mutant TRPMLs. Wild-type TRPV5 and TRPV6 are highly Ca^{2+}-selective, display constitutive activity, and show substantial Ca^{2+}-dependent inactivation (22, 23), which is in contrast to the TRPML channels, which are closed under comparable conditions. We hypothesize that the proline

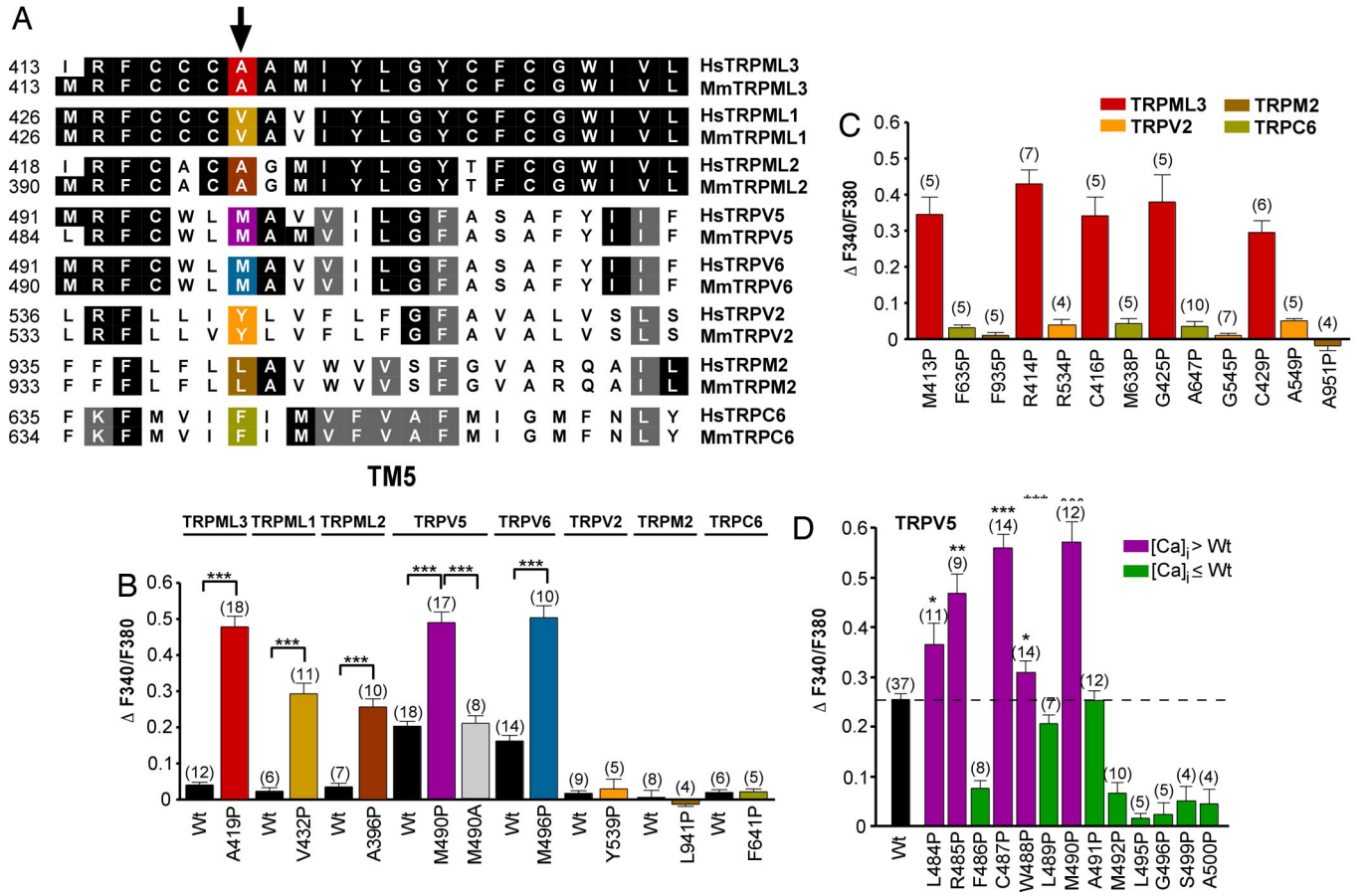

Fig. 4. Susceptibility to proline substitutions in TM5 is a general feature of TRPML channels as well as TRPV5 and TRPV6. (*A*) Amino acid sequence comparison of TM5 of human (Hs) and murine (Mm) TRPML3 with TRPML1, TRPML2, TRPV5, TRPV6, TRPV2, TRPM2, and TRPC6. Positions equivalent to TRPML3(A419P) (red) are highlighted: yellow, TRPML1; dark brown, TRPML2; magenta, TRPV5; blue, TRPV6; orange, TRPV2; brown, TRPM2; olive, TRPC6. (*B*) Relative $[Ca^{2+}]_i$ levels of HEK293 cells expressing mmTRPML3, hsTRPML1, mmTRPML2, mmTRPV5, mmTRPV6, mmTRPV2, hsTRPM2, and hsTRPC6 wild type and mutant isoforms as indicated in *A*. Shown are mean values ± SEM with the number of independent experiments with at least 5–10 cells each shown in parentheses. (*C*) Proline substitutions at additional positions in TM5 of TRPV2, TRPM2, and TRPC6. Proline substitutions of TRPML3 at equivalent positions resulted in elevated $[Ca^{2+}]_i$ (red bars). None of the mutated TRPV2, TRPM2, and TRPC6 isoforms displayed elevated $[Ca^{2+}]_i$. (*D*) Effect on $[Ca^{2+}]_i$ of proline substitution along TM5 of murine TRPV5. Shown are mean values ± SEM with *n* in parentheses. ***, $P < 0.0001$; **, $P < 0.001$; *, $P < 0.05$ (Student's *t* test, unpaired, comparison with wild type).

substitutions in TM5 alter Ca^{2+}-dependent inactivation either directly to leave the channel constitutively active or indirectly by altering the channel pore in a manner that reduces the effectiveness of inactivation.

It is not intuitively obvious why a mutation in TM5 would affect activity of TRPML3 because it has been postulated that the pore-forming and pore-lining domains of TRP channels are located downstream of TM5 (24, 25). Nevertheless, proline- or glycine-mediated kinks or swivels in α-helices of ion channels can play roles in ion channel function (10, 26, 27). For example, proline or glycine swivels in the pore-lining helix TM2 of the inward rectifier potassium channels of the GIRK family have profound effects on its open probability (28, 29). Likewise, a swivel motion of a glycine in the M2 helix of KcsA, which is equivalent to TM2 of GIRK, is involved in conformational fluctuations (30, 31), and glycine and proline-based hinges in the S6 transmembrane segment of *Shaker*-type K^+ channels play important functional roles in determining the pore features (27, 32). Furthermore, interactions of the intracellular regions of other transmembrane-spanning domains with TM6 have been shown to be critical for activation gating in some potassium channels (33, 34). Our observation that proline substitutions in TM5 of TRPML3 lead to constitutive activity suggest that the mutation causes structural changes affecting important properties of the channel. Without knowledge of the biophysical features of wild-type TRPML3, it is difficult to investigate whether these changes alter activation gating or conductivity. Toward this goal, we attempted to activate wild-type TRPML3 in a variety of ways, including osmolality changes, mechanical stimulation, pH, and varying intracellular calcium buffering as well as extracellular calcium, all without success. Future directions, consequently, need to address whether TRPML3 is an activatable ion channel in hair cells, intermediate cells, or other cell types that natively express the protein.

Materials and Methods

Calcium Imaging and HEK293 Cell Electrophysiology. Measurements using the fluorescent indicators fura-2-AM and SBFI-AM (Invitrogen) were performed by using the iMic platform and Polychrome V monochromator (TILL Photonics).

Whole-cell currents were recorded 12–15 h after transfection with an Axopatch 200B amplifier and acquired with JClamp software. Standard bath solution contained 138 mM NaCl, 5.4 mM KCl, 2 mM $MgCl_2$, 2 mM $CaCl_2$, 10 mM Hepes, and 10 mM D-glucose (pH 7.4). Pipette solution contained 140 mM CsCl, 10 mM Hepes, 3 mM ATP-Na, 1 mM BAPTA, and 2 mM $MgCl_2$ (pH 7.2). Series resistance was 1.8 ± 0.4 MΩ (n = 21), after compensation, and capacitance was 5.5 ± 0.7 pF. Stock solutions

(100 mM) of ADP-ribose, DPBA (both from Sigma), and DDG (Biomol) were prepared in DMSO. 2-Aminoethyl-diphenyl borate (2-APB; 100 μM) was included in the bath solution to block gap junctions. 2-APB had no effect on the expressed channels.

Hair Cell Electrophysiology. Animal studies were conducted under institutionally approved animal study protocols using standards set forth by the National Institutes of Health and the U.K. Home Office. OHCs from varitint-waddler mutant (Va^J/Va^J) and matching control (+/+) mice were studied after acute dissection of the organ of Corti (P3–P5). Additional details are provided in *SI Methods*.

Biotinylation and Western Blots. Sample preparation and processing for Western blot analysis were conducted as previously described (35). A detailed description of the biotinylation protocol is provided in *SI Methods*.

Additional Details. Additional methods and more details are included in *SI Methods*.

We thank the members of our laboratories for providing valuable comments on the manuscript. We also thank Drs. Konrad Noben-Trauth and Guy Richardson for helpful discussions, and we are grateful to three anonymous reviewers for their helpful suggestions. This work was supported by Human Frontier Science Program Research Grant RPG0032/2004 and National Institutes of Health Grant DC04563 (to S.H.), National Institutes of Health Grant DC08396 (to A.J.R.), a Medical Research Council Program Grant (to C.J.K), and EuroHear, an EU Integrated Project (C.J.K.).

1. Clapham DE (2003) *Nature* 426:517–524.
2. Montell C (2005) *Sci STKE* 2005, re3.
3. Walker RG, Willingham AT, Zuker CS (2000) *Science* 287:2229–2234.
4. Kim J, Chung YD, Park DY, Choi S, Shin DW, Soh H, Lee HW, Son W, Yim J, Park CS, *et al.* (2003) *Nature* 424:81–84.
5. Gong Z, Son W, Chung YD, Kim J, Shin DW, McClung CA, Lee Y, Lee HW, Chang DJ, Kaang BK, *et al.* (2004) *J Neurosci* 24:9059–9066.
6. Bargal R, Avidan N, Ben-Asher E, Olender Z, Zeigler M, Frumkin A, Raas-Rothschild A, Glusman G, Lancet D, Bach G (2000) *Nat Genet* 26:118–123.
7. Bach G (2005) *Pflügers Arch* 451:313–317.
8. Di Palma F, Belyantseva IA, Kim HJ, Vogt TF, Kachar B, Noben-Trauth K (2002) *Proc Natl Acad Sci USA* 99:14994–14999.
9. Cable J, Steel KP (1998) *Hear Res* 123:125–136.
10. Sansom MS, Weinstein H (2000) *Trends Pharmacol Sci* 21:445–451.
11. Ri Y, Ballesteros JA, Abrams CK, Oh S, Verselis VK, Weinstein H, Bargiello TA (1999) *Biophys J* 76:2887–2898.
12. Chung MK, Guler AD, Caterina MJ (2005) *J Biol Chem* 280:15928–15941.
13. Grimm C, Kraft R, Schultz G, Harteneck C (2005) *Mol Pharmacol* 67:798–805.
14. Hofmann T, Obukhov AG, Schaefer M, Harteneck C, Gudermann T, Schultz G (1999) *Nature* 397:259–263.
15. Perraud AL, Fleig A, Dunn CA, Bagley LA, Launay P, Schmitz C, Stokes AJ, Zhu Q, Bessman MJ, Penner R, *et al.* (2001) *Nature* 411:595–599.
16. Kraft R, Grimm C, Grosse K, Hoffmann A, Sauerbruch S, Kettenmann H, Schultz G, Harteneck C (2004) *Am J Physiol* 286:C129–C137.
17. Edmonds B, Reyes R, Schwaller B, Roberts WM (2000) *Nat Neurosci* 3:786–790.
18. Heller S, Bell AM, Denis CS, Choe Y, Hudspeth AJ (2002) *J Assoc Res Otolaryngol* 3:488–498.
19. Hackney CM, Mahendrasingam S, Penn A, Fettiplace R (2005) *J Neurosci* 25:7867–7875.
20. Yamoah EN, Lumpkin EA, Dumont RA, Smith PJ, Hudspeth AJ, Gillespie PG (1998) *J Neurosci* 18:610–624.
21. Dumont RA, Lins U, Filoteo AG, Penniston JT, Kachar B, Gillespie PG (2001) *J Neurosci* 21:5066–5078.
22. Nilius B, Weidema F, Prenen J, Hoenderop JJ, Vennekens R, Hoefs S, Droogmans G, Bindels RM (2003) *Pflügers Arch* 445:584–588.
23. Mensenkamp AR, Hoenderop JG, Bindels RJ (2007) *Handb Exp Pharmacol* 179:207–220.
24. Voets T, Nilius B (2003) *Cell Calcium* 33:299–302.
25. Nilius B, Watanabe H, Vriens J (2003) *Pflügers Arch* 446:298–303.
26. Tieleman DP, Shrivastava IH, Ulmschneider MR, Sansom MS (2001) *Proteins* 44:63–72.
27. Labro AJ, Raes AL, Bellens I, Ottschytsch N, Snyders DJ (2003) *J Biol Chem* 278:50724–50731.
28. Jin T, Peng L, Mirshahi T, Rohacs T, Chan KW, Sanchez R, Logothetis DE (2002) *Mol Cell* 10:469–481.
29. Sadja R, Smadja K, Alagem N, Reuveny E (2001) *Neuron* 29:669–680.
30. Jiang Y, Lee A, Chen J, Cadene M, Chait BT, MacKinnon R (2002) *Nature* 417:523–526.
31. Holyoake J, Domene C, Bright JN, Sansom MS (2004) *Eur Biophys J* 33:238–246.
32. Ding S, Ingleby L, Ahern CA, Horn R (2005) *J Gen Physiol* 126:213–226.
33. Long SB, Campbell EB, Mackinnon R (2005) *Science* 309:903–908.
34. Lu Z, Klem AM, Ramu Y (2002) *J Gen Physiol* 120:663–676.
35. Cuajungco MP, Grimm C, Oshima K, D'Hoedt D, Nilius B, Mensenkamp AR, Bindels RJ, Plomann M, Heller S (2006) *J Biol Chem* 281:18753–18762.